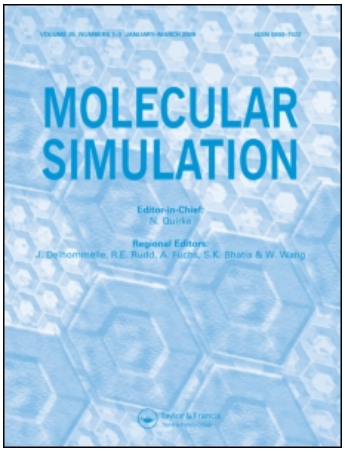

Molecular Simulation
Publication details, including instructions for authors and subscription information:
http://www.informaworld.com/smpp/title~content=t713644482

Electronic structure and charge ordering in magnetite: implications for the Fe_3O_4 (001)-water interface

Sándor Á. Kovács[a]; Cynthia S. Lo[a]
[a] Department of Energy, Environmental and Chemical Engineering, Washington University in St Louis, St Louis, MO, USA

First published on: 09 November 2010

To cite this Article Kovács, Sándor Á. and Lo, Cynthia S.(2010) 'Electronic structure and charge ordering in magnetite: implications for the Fe_3O_4 (001)-water interface', Molecular Simulation, 36: 15, 1289 — 1296, First published on: 09 November 2010 (iFirst)
To link to this Article: DOI: 10.1080/08927022.2010.517735
URL: http://dx.doi.org/10.1080/08927022.2010.517735

Molecular Simulation
Vol. 36, No. 15, December 2010, 1289–1296

Taylor & Francis
Taylor & Francis Group

Electronic structure and charge ordering in magnetite: implications for the Fe_3O_4 (001)–water interface

Sándor Á. Kovács and Cynthia S. Lo*

Department of Energy, Environmental and Chemical Engineering, Washington University in St Louis, St Louis, MO, USA

(*Received 15 September 2009; final version received 19 August 2010*)

Electronic structure calculations on atomistic models of magnetite (Fe_3O_4) provide valuable insight into the structure and properties that dictate the behaviour of magnetite under environmental conditions. The charge ordering in the bulk oxide controls the reactivity of the exposed surfaces, but it has been difficult to measure experimentally or predict theoretically. We use spin-polarised density functional theory to calculate the structure of bulk Fe_3O_4 and its (001) and (111) surface terminations. We then present an *ab initio* thermodynamics approach to determine the most energetically favourable clean and hydroxylated surface terminations of Fe_3O_4 (001). We present results on molecular water adsorption and heterolytic dissociation at both quarter- and half-monolayer coverage for Fe_3O_4 (001). Our calculations suggest that the tetrahedral (001) surface termination is the most energetically stable across all oxygen chemical potentials, and that water molecules preferentially dissociate at the surface. The calculated hydroxylated and hydrated surface terminations, as obtained from careful consideration of the charge ordering in the bulk, serve as a strong basis for future studies of the electrical double layer at the mineral–water interface.

Keywords: magnetite; Fe_3O_4; density functional theory; charge ordering; interface

1. Introduction

Electronic structure calculations using the density functional theory (DFT) [1,2] approach have provided valuable insight into the magnetite system [3,4]. Magnetite occurs naturally as a ferrimagnetic material with a net magnetic moment due to the presence of both Fe^{2+} and Fe^{3+} in the unit cell [5]. With a formula unit of Fe_3O_4 and a 56-atom unit cell consisting of eight of these units, magnetite belongs to the family of AX_2B_4 spinel materials. At higher temperatures, magnetite naturally assumes an inverse spinel structure with the higher oxidation states (3+) occupying all the octahedral sites [6]. However, at temperatures below the Verwey transition [7] at 177 K, the charge ordering changes and Fe^{3+} is found in both tetrahedral and octahedral sites [8]. Since it is presumed that charge ordering in the bulk oxide controls the reactivity of the exposed surfaces, it is vitally important to determine the spatial arrangement of Fe^{2+} and Fe^{3+} among the octahedral sites.

Unfortunately, the exact assignment of these charges in the bulk oxide has proved elusive. Many experimental approaches, such as X-ray and neutron diffraction, have been used to glean charge-ordering information and have met with varying levels of success [9,10]. Thus, the importance of the exact structure of the bulk material is often ignored in favour of focusing on surface reconstructions [11] and interactions with other species [12–16]. An early approach to modelling the bulk material using a local density approximation (LDA) led to an overall metallic state with octahedral sites occupied by iron atoms in a +2.5 oxidation state, inconsistent with available data [17]. More recent modelling studies have used either self-interactions corrected LDA or LDA + U methods, but lack accuracy because of the minimal basis sets required for such calculations to converge [18–20].

In order to avoid this shortcoming, the DFT approach used in this work uses a plane wave basis set implemented as part of the generalised gradient approximation (GGA). Beginning from a more rigorous treatment of the system by considering the two charge assignments of Verwey as well as nine additional charge assignments based on symmetry rules [21] for the inverse-spinel structure, 11 bulk charge assignments are considered in total [22]. These models have the advantage of treating the bulk phase more precisely, as a 224-atom supercell with P1 symmetry is required instead of the conventional 56-atom unit cell with high symmetry. This requirement not only enables the construction of the 11 models, but also allows for subtle variations in the atomic position difficult to explore using other methods. After establishing the charge-ordering of the bulk material, this work presents an updated representation of the (001) and (111) magnetite surfaces and investigates the interaction of water with the (001) surface.

*Corresponding author. Email: clo@wustl.edu

ISSN 0892-7022 print/ISSN 1029-0435 online

DOI: 10.1080/08927022.2010.517735
http://www.informaworld.com

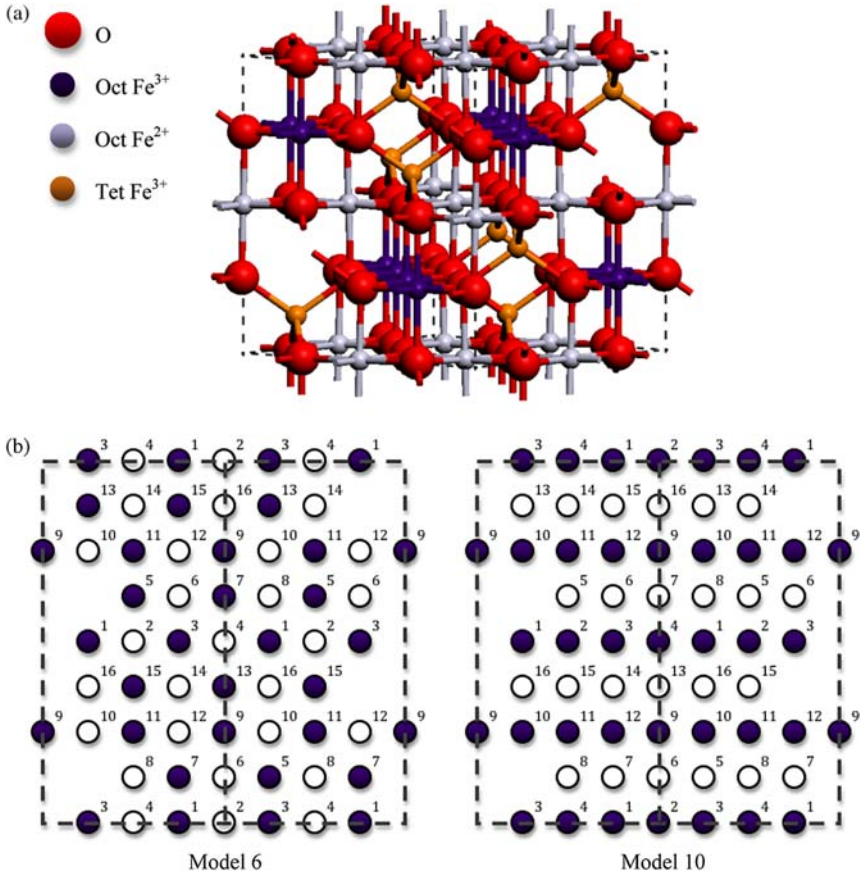

Figure 1. (a) The 56-atom unit cell of magnetite rotated to display inverse-spinel structure. Oxygen atoms are large and shown in red, octahedral iron atoms are smaller and shown in purple, tetrahedral Fe^{3+} iron atoms are small and shown in orange. Alternating layers of Fe^{2+} and Fe^{3+} corresponding to the Verwey structure, are shown in light and dark purple, respectively. (b) Site assignments for 224-atom supercell Model 6 (left) and Model 10 (right) as viewed along the (110) direction. Sites have been numbered according to Table 1 and only octahedral irons are shown for clarity. Fe^{2+} and Fe^{3+} ions are shown as light and dark (purple) spheres, respectively (colour online).

2. Method

2.1 Model development

In order to investigate the issue of charge ordering via *ab initio* modelling, the conventional 56-atom unit cell of magnetite as shown in Figure 1(a) is inadequate. Instead, the 56-atom unit cell of magnetite is redefined along original lattice vectors $[\mathbf{a}] = [\sqrt{2}\ \sqrt{2}\ 0]$, $[\mathbf{b}] = [\sqrt{2}\ -\sqrt{2}\ 0]$ and $[\mathbf{c}] = [0\ 0\ 2]$ to create a supercell four times the size, containing 224 atoms. The additional atoms allow for the consideration of complex charge assignments, as described by the site number in Table 1 and exemplified in Figure 1(b).

2.2 DFT parameters

Spin-polarised DFT [5] calculations were performed using the CASTEP [23] code to determine the electronic structure and properties of the systems considered in this study. The electron exchange and correlation energies were calculated using the GGA of Perdew, Burke and Ernzerhof [24,25] and core electrons were treated using Vanderbilt ultrasoft pseudopotentials [26]. Calculations were performed with an initial spin multiplicity estimated from the number of irons in the bulk unit cell. Geometry optimisations were performed with an energy tolerance of 2×10^5 eV/atom, an atomic displacement tolerance of 2×10^{-3} Å, a force tolerance of 5×10^{-2} eV/Å, a maximum stress component tolerance of 0.1 GPa, a plane wave cut-off of 300 eV and a convergence tolerance of two iterations. Spin-unrestricted calculations and sufficiently high cut-off energies guarantee the stability of the wave function. All calculations used periodic boundary conditions, and both (001) and (111) surfaces were modelled as semi-infinite slabs with >15 Å of vacuum between slabs.

2.3 Hydrated surfaces

Once the geometry optimisations of the low-index surface models were complete and slab surfaces checked for consistency, water was added to the system. One formula unit or two formula units of water were added to top and bottom (001) surfaces, representing quarter- and

Table 1. The octahedral site charge assignments for the 11 bulk models considered in this study.

	Octahedral site charge assignment																
Model	1	2	3	4	5	6	7	8	9	10	11	12	13	14	15	16	Energy (meV)
1	3	2	2	2	3	2	3	3	2	2	3	2	3	3	2	3	+3.16
2	3	2	2	2	3	2	3	3	2	3	2	2	3	3	3	2	+3.05
3	3	3	3	2	3	2	2	2	2	3	3	3	3	2	2	2	+3.03
4	3	3	3	2	3	2	2	2	3	3	3	2	2	3	2	2	+4.38
5	3	2	2	3	2	2	3	3	2	2	3	3	3	2	2	3	+2.76
6	3	2	3	2	3	2	3	2	3	2	3	2	3	2	3	2	+10.34
7	3	2	2	3	2	2	3	3	3	2	3	2	3	2	3	2	+0.66
8	3	3	2	2	3	2	3	2	3	2	3	2	3	3	2	2	+15.29
9	3	2	3	2	2	3	3	2	3	2	2	3	3	2	3	2	+0.152
10	**2**	**2**	**2**	**2**	**3**	**3**	**3**	**3**	**2**	**2**	**2**	**2**	**3**	**3**	**3**	**3**	**+0.00**
11	3	3	3	3	2	2	2	2	3	3	3	3	2	2	2	2	+11.86

Note: All tetrahedral sites contained Fe^{3+}. Each model's energy has been normalised with respect to Model 10 to highlight the slight differences the charge assignment creates.

half-monolayer coverage, respectively. These water molecules were either adsorbed molecularly or dissociated heterolytically at under-coordinated iron sites by attaching hydroxyl (R-OH) groups. A second series of geometry optimisations determined hydrated surface energies, γ, according to the following equation:

$$\gamma = \frac{1}{2A}\left[E^{\text{slab}} - N_{\text{Fe}}\mu_{\text{Fe}} - N_{\text{O}}\mu_{\text{O}} - N_{\text{H}}\mu_{\text{H}}\right],$$

where A is the surface area, E^{slab} is the result of the energy calculation, N_i represents the number of atoms of a species i and μ_i represents the chemical potential of species i. The following assumptions are made:

$$\mu_{Fe_3O_4} = 3\mu_{\text{Fe}} + 4\mu_{\text{O}} \quad \text{and} \quad \mu_{H_2O} = 2\mu_{\text{H}} + \mu_{\text{O}}.$$

The surface energy expression can be rewritten in terms of available quantities

$$\gamma = \frac{1}{2A}\left[E^{\text{slab}} - \frac{N_{\text{Fe}}}{3}(\mu_{Fe_3O_4} - 4\mu_{\text{O}}) - N_{\text{O}}\mu_{\text{O}} - \frac{N_{\text{H}}}{2}(\mu_{H_2O} - \mu_{\text{O}})\right].$$

Next, terms are grouped with respect to the calculated energies of bulk magnetite and water, with the oxygen

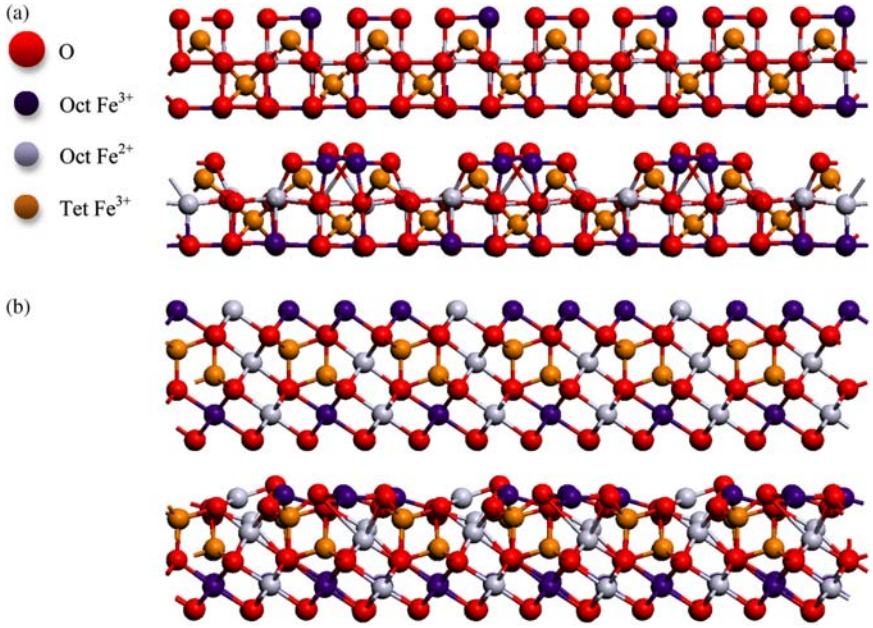

Figure 2. (a) Structure of the stoichiometric (001) octahedral surface of magnetite before and after geometry optimisation. With the charge ordering taken into account, the surface undergoes a predictable Jahn–Teller reconstruction, relaxing the under-coordinated atoms to form a ridged or wave-like structure. (b) Structure of the stoichiometric (111) octahedral surface of magnetite before and after geometry optimisation. The under-coordinated surface iron atoms in the octahedral sites have relaxed well into the oxygen layer beneath, forming a passivated surface (colour online).

Table 2. Energies of the four stoichiometric magnetite surfaces considered in this study.

System	Lattice parameters (Å)			Surface energy (meV/Å^2)
	a	*b*	*c*	
(001) Tetrahedral	8.494	8.494	16.892	+32.18
(001) Octahedral				+61.96
(111) Octahedral	11.979	11.979	9.789	+40.67
(111) Tetrahedral				+38.14

Note: Slab energy was calculated for each configuration and then normalised to a 56-atom unit cell. The normalised surface energy was calculated by dividing the slab energy by the surface area, as calculated from the optimised lattice parameters.

chemical potential left as variable:

$$\gamma = \frac{1}{2A}\left[E^{\text{slab}} - \frac{N_{\text{Fe}}}{3}\left(G^{\text{bulk}}_{\text{Fe}_3\text{O}_4}\right) - \frac{N_{\text{H}}}{2}\left(G^{\text{bulk}}_{\text{H}_2\text{O}}\right) + \left(\frac{4N_{\text{Fe}}}{3} - N_{\text{O}} + \frac{N_{\text{H}}}{2}\right)\mu_{\text{O}}\right].$$

However, since all the surfaces considered were stoichiometric, the μ_{O} term reduces to zero in each case. From the results of these calculations, a phase diagram for the magnetite–water system dependent on the chemical potential of oxygen can be constructed.

3. Results

The energies of each of the 11 investigated magnetite bulk models with the site-specific numbering system shown in

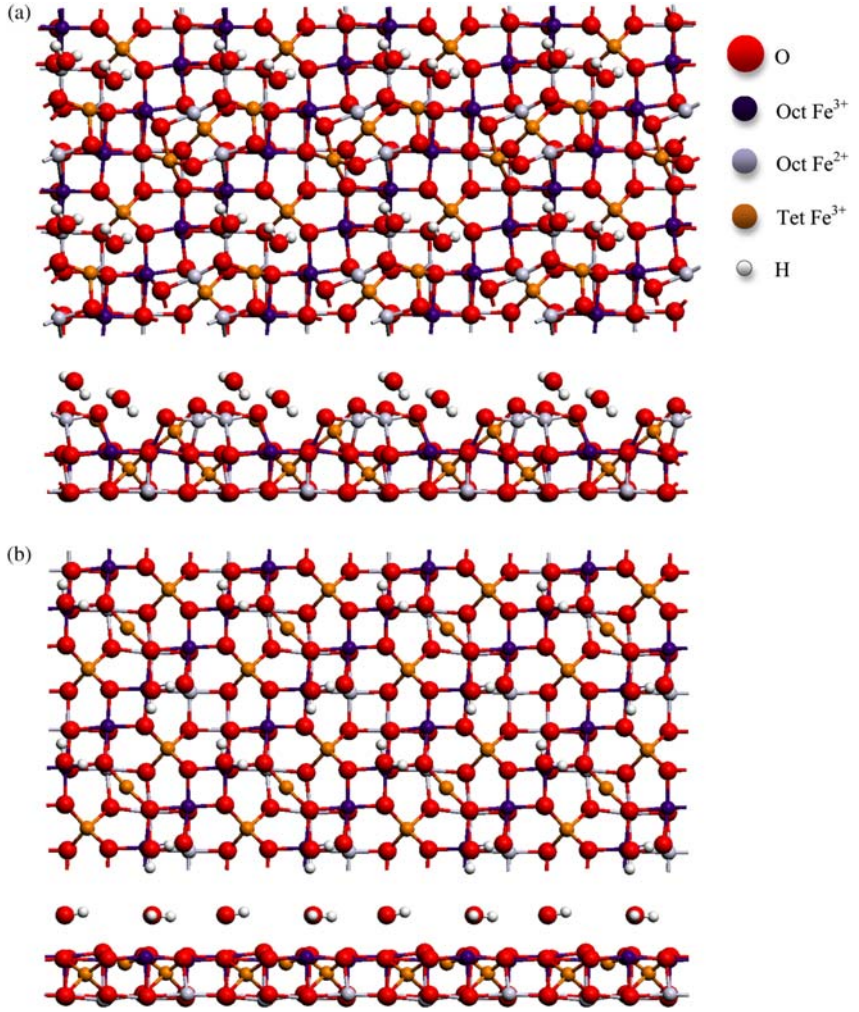

Figure 3. (a) Absorbed water molecules on the octahedral (001) surface, from above and from the side. Strong hydrogen bonds form between surface oxygen atoms and the hydrogen atoms of water molecules. (b) Absorbed water molecules on the tetrahedral (001) surface, from above and from the side. The presence of the water molecules on the surface causes the under-coordinated tetrahedral iron atoms to relax, forming a passivated oxygen layer (colour online).

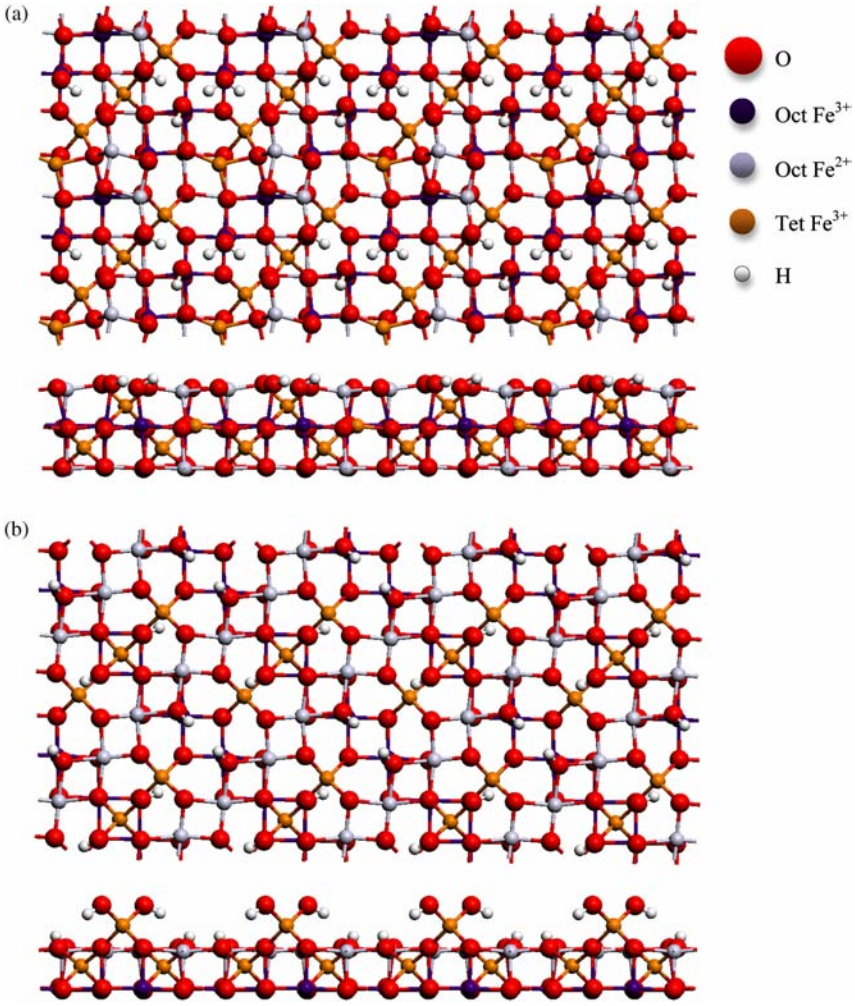

Figure 4. (a) Dissociated water molecules on the octahedral (001) surface, from above and from the side. (b) Dissociated water molecules on the tetrahedral (001) surface, from above and from the side. The hydroxyl groups fill empty orbitals of the iron atoms, returning them to an octahedral coordination and lowering surface energy. Hydrogen bonding between hydroxyl and hydride groups helps to stabilise the surface reconstruction (colour online).

Figure 1(b) are presented in Table 1. Model 10, which features alternating layers of Fe^{2+} and Fe^{3+}, was found to have the lowest energy. Fittingly, this model is in accordance with Verwey's original prediction in 1939, and has been confirmed, to the best of the authors' knowledge, for the first time in this work. The spins imparted on the system remained consistent with originally assigned directions, but changes in their magnitude were observed, as they relaxed from $+4$ or $\pm 5\,\mu B$ to $\pm 1.8\,\mu B$. The spin moment of the oxygen atoms also increased slightly, to $+0.05\,\mu B$; analogous findings have also been reported in the literature [27]. Based on the optimised supercell system, an updated 56-atom unit cell structure was created for comparison. This 56-atom unit cell has optimised lattice parameters $a = 8.494$ Å, $b = 8.494$ Å and $c = 8.446$ Å, which represent a slight relaxation from experimental values [8].

Starting from the optimised alternating layer model of the magnetite bulk, (001) and (111) surfaces were created with octahedral and tetrahedral terminations, for a total of four surface models. These surface models consisted of two stacked unit cells, for a total of 112 atoms. Representative results for two of these four surfaces may be seen in Figure 2(a) and (b). Optimised lattice parameters and surface energies normalised for surface area are reported in Table 2.

The spins of the iron atoms in the surface models also exhibited relaxation from their bulk assignments, and again did not change in direction. In the case of the (001) octahedral surface, oxygen spins ranged from -0.17 to $+0.22\,\mu B$, while iron spins ranged from -1.41 to $-1.81\,\mu B$ for the spin down octahedral sites and $+1.24$ to $+1.90\,\mu B$ for the spin up octahedral and tetrahedral sites. The under-coordinated atoms at the slab surface had a greater degree of spin relaxation from the bulk assignment.

Table 3. Surface energies of the eight hydrated terminations of the Fe_3O_4 (001) surface found in this study.

		Surface energies (meV/Å^2)		
System	Description	# H_2O	Adsorbed	Dissociated
(001)	Vacuum	0	+32.18	
Tetrahedral	Quarter-monolayer	1	+26.74	+19.50
	Half-monolayer	2	+24.53	+16.09
(001)	Vacuum	0	+61.96	
Octahedral	Quarter-monolayer	1	+44.03	+47.74
	Half-monolayer	2	+32.80	+26.03

Note: Bare surface results have been reprinted for comparison. Adsorbed configurations were modelled by the addition of the corresponding number of water molecules 2 Å above the surface, while adding hydroxide and hydride groups to under-coordinated iron and oxygen atoms modelled dissociated configurations. Sample surface models can be seen in Figures 3 and 4.

This phenomenon is known as spin canting and has been observed for magnetite surface models [28], but has not, to the authors' knowledge, been reported to this level of detail.

Finally, the tetrahedral and octahedral surface terminations were each hydrated to quarter- and half-monolayer coverage, in order to determine the behaviour of these surfaces under environmental conditions. Two treatments of water were considered: molecular adsorption and heterolytic dissociation. Optimised surface terminations resulting from water adsorption and dissociation at half-monolayer coverage are depicted in Figures 3 and 4, respectively, and are reported for the 10 surface terminations listed in Table 3. Overall, the processes of hydration and hydroxylation led to a decrease in surface energy due to favourable enthalpic interactions. In several cases, strong hydrogen bonds are observed between the oxygen atoms on the oxide surface and the hydrogen atoms in the adsorbed or dissociated waters. Additionally, water dissociation is favoured energetically relative to molecular adsorption. In all cases, the tetrahedral termination was more energetically favourable than the corresponding octahedral termination. These results are summarised in the phase diagram for dissociated waters shown in Figure 5.

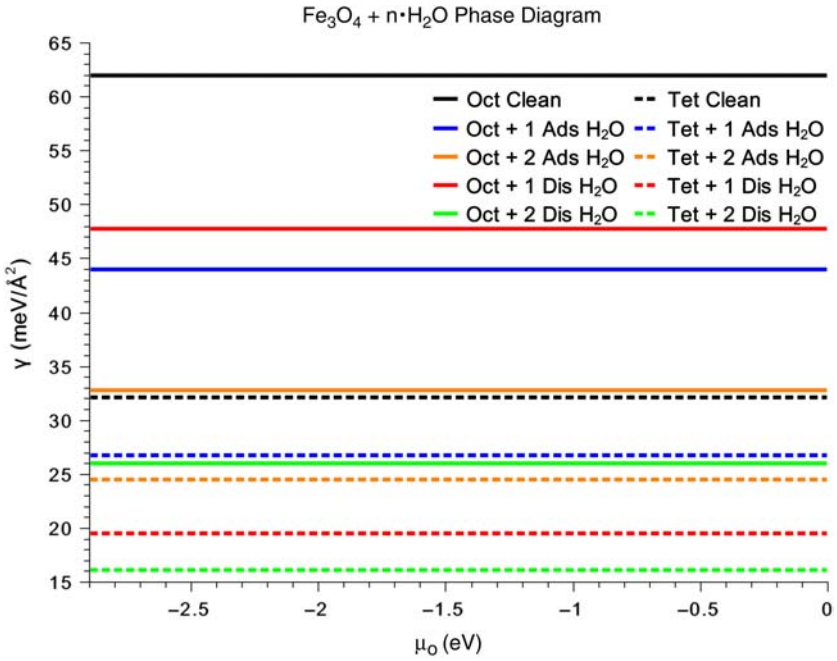

Figure 5. Phase diagram for water interacting with the (001) magnetite surface. Solid lines represent octahedral termination; dashed lines represent the tetrahedral termination. Oxygen chemical potential is varied from −2.9 eV corresponding to the oxygen in Fe_3O_4 to 0.0 eV, corresponding to elemental O_2 (colour online).

4. Discussion

In comparison with previously published studies on magnetite surfaces [8,29–32], the surface termination models presented in this study follow the same procedure, where the bulk oxide is used as a starting point for cleaving semi-infinite slab models of the surface. Nevertheless, the main difference between our findings and those previously published for both the (001) and (111) surfaces is that in this study, the charge ordering considered in the bulk was retained in the surface models. Recent modelling results on Fe_3O_4 (001) agree that increased hydration is energetically favoured, but suggest that an octahedral termination is the preferred or observed (001) surface termination at the mineral–water interface [33,34]. It is unclear if the impact of the bulk charge ordering was considered in that work, which suggests the need for future studies on the nature of the electrical double layer.

Furthermore, the details of the spin canting observed in the system, responsible for the relaxations observed in μB, are beyond the scope of the present study. Future studies may explore this issue by using an even more accurate description of the electronic structure, such as one provided by a linear augmented plane wave DFT code with a sufficiently large basis set size.

5. Conclusions

The structure and energetics of charge-ordered bulk magnetite and surface terminations of Fe_3O_4 (001) and (111) have been calculated. The (001) surface terminated by tetrahedral iron atoms is the lowest energy stoichiometric surface resulting from these charge-ordered calculations. Magnetite (001) also preferentially dissociates water at its under-coordinated iron cations compared to adsorbing water molecularly. Thus, the most favourable surface termination consists of the (001) surface tetrahedral iron atoms fully coordinated with heterolytically dissociated water molecules. The hydrated (001) and optimised (111) surface geometries based on the charge-ordered bulk structure developed in this study provide an accurate basis for future studies of environmental reactivity.

References

[1] P. Hohenberg and W. Kohn, *Inhomogeneous electron gas*, Phys. Rev. 136(3B) (1964), pp. B864–B871.

[2] W. Kohn and L.J. Sham, *Self-consistent equations including exchange and correlation effects*, Phys. Rev. 140(4A) (1965), pp. A1133–A1138.

[3] R. Pentcheva, W. Moritz, J. Rundgren, S. Frank, D. Schrupp, and M. Scheffler, *A combined DFT/LEED-approach for complex oxide surface structure determination: Fe_3O_4 (0 0 1)*, Surf. Sci. 602(7) (2008), pp. 1299–1305.

[4] U. Diebold, *Wiggling its way out of surface polarity: Fe_3O_4 (1 0 0) (A perspectives on the article: 'A combined DFT/LEED approach for complex oxide surface structure determination: Fe_3O_4 (0 1 1)' by R. Pentcheva, W. Moritz, J. Rundgren, S. Frank, D. Schrupp, M. Scheffler)*, Surf. Sci. 602(7) (2008), pp. 1297–1298.

[5] J.M. Zuo, J.C.H. Spence, and W. Petuskey, *Charge ordering in magnetite at low temperatures*, Phys. Rev. B 42(13) (1990), pp. 8451–8464.

[6] Z. Zhang and S. Satpathy, *Electron states, magnetism, and the Verwey transition in magnetite*, Phys. Rev. B 44(24) (1991), pp. 13319–13331.

[7] E.J.W. Verwey, *Electronic conduction of magnetite (Fe_3O_4) and its transition point at low temperature*, Nature 144 (1939), pp. 327–328.

[8] M. Fonin, Y.S. Dedkov, R. Pentcheva, U. Rudiger, and G. Guntherodt, *Magnetite: A search for the half-metallic state*, J. Phys. Condens. Matter 19(31) (2007), p. 315217.

[9] J. Garcìa, G. Subìas, M.G. Proietti, J. Blasco, H. Renevier, J.L. Hodeau, and Y. Joly, *Absence of charge ordering below the Verwey transition temperature in magnetite*, Phys. Rev. B 63(5) (2001), 054110.

[10] J.P. Wright, J.P. Attfield, and P.G. Radaelli, *Long range charge ordering in magnetite below the Verwey transition*, Phys. Rev. Lett. 87(26) (2001), 266401.

[11] R.J. McQueeney, M. Yethiraj, W. Montfrooij, J.S. Gardner, P. Metcalf, and J.M. Honig, *Investigation of the presence of charge order in magnetite by measurement of the spin wave spectrum*, Phys. Rev. B 73(17) (2006), 174409.

[12] J.R. Rustad, E. Wasserman, and A.R. Felmy, *A molecular dynamics investigation of surface reconstruction on magnetite (001)*, Surf. Sci. 432(1–2) (1999), pp. L583–L588.

[13] Z.X. Sun, F.W. Su, W. Forsling, and P.O. Samskog, *Surface characteristics of magnetite in aqueous suspension*, J. Colloid Interface Sci. 197(1) (1998), pp. 151–159.

[14] T. Kendelewicz, P. Liu, C.S. Doyle, G.E. Brown, E.J. Nelson, and S.A. Chambers, *Reaction of water with the (100) and (111) surfaces of Fe_3O_4*, Surf. Sci. 453(1–3) (2000), pp. 32–46.

[15] J.R. Rustad, A.R. Felmy, and E.J. Bylaska, *Molecular simulation of the magnetite–water interface*, Geochim. Cosmochim. Acta 67(5) (2003), pp. 1001–1016.

[16] T. Yang, X.D. Wen, C.F. Huo, Y.W. Li, J. Wang, and H. Jiao, *Structure and energetics of hydrogen adsorption on Fe_3O_4 (111)*, J. Mol. Catal. A Chem. 302(1–2) (2009), pp. 129–136.

[17] T. Yang, *Structures and energetics of H_2O adsorption on the Fe_3O_4 (111) surface*, J. Fuel Chem. Technol. 37(4) (2009), pp. 506–512.

[18] V.I. Anisimov, I.S. Elfimov, N. Hamada, and K. Terakura, *Charge-ordered insulating state of Fe_3O_4 from first-principles electronic structure calculations*, Phys. Rev. B 54(7) (1996), pp. 4837–4890.

[19] Z. Szotek, W.M. Temmerman, A. Svane, L. Petit, G.M. Stocks, and H. Winter, Ab initio *study of charge order in Fe_3O_4*, Phys. Rev. B 68(5) (2003), 054415.

[20] G.K. Madsen and P. Novak, *Charge order in magnetite. An LDA + U study*, Europhys. Lett. 69 (2005), pp. 777–783.

[21] M.E. Grillo, M.W. Finnis, and W. Ranke, *Surface structure and water adsorption on Fe_3O_4 (111): Spin-density functional theory and on-site Coulomb interactions*, Phys. Rev. B 77 (2008), 075407.

[22] P.W. Anderson, *Localized magnetic states in metals*, Phys. Rev. 124(1) (1961), pp. 41–53.

[23] R.G. Parr, *Density functional theory*, Annu. Rev. Phys. Chem. 34(1) (1983), pp. 631–656.

[24] M.D. Segall, P.J.D. Lindan, M.J. Probert, C.J. Pickard, P.J. Hasnip, S.J. Clark, and M.C. Payne, *First-principles simulation: Ideas, illustrations and the CASTEP code*, J. Phys.: Condens. Matter 14(11) (2002), pp. 2717–2743.

[25] J.P. Perdew, K. Burke, and Y. Wang, *Generalized gradient approximation for the exchange-correlation hole of a many-electron system*, Phys. Rev. B Condens. Matter 54(23) (1996), pp. 16533–16539.

[26] M. Ernzerhof and G.E. Scuseria, *Assessment of the Perdew–Burke–Ernzerhof exchange-correlation functional*, J. Chem. Phys. 110 (1999), pp. 5029–5036.

[27] K. Laasonen, R. Car, C. Lee, and D. Vanderbilt, *Implementation of ultrasoft pseudopotentials in* ab initio *molecular dynamics*, Phys. Rev. B 43(8) (1991), pp. 6796–6799.

[28] V.S. Zaitsev, D.S. Filimonov, I.A. Presnyakov, R.J. Gambino, and B. Chu, *Physical and chemical properties of magnetite and*

magnetite-polymer nanoparticles and their colloidal dispersions, J. Colloid Interface Sci. 212(1) (1999), pp. 49–57.
[29] B. Stanka, W. Hebenstreit, U. Diebold, and S.A. Chambers, *Surface reconstruction of Fe_3O_4 (001)*, Surf. Sci. 448(1) (2000), pp. 49–63.
[30] I.V. Shvets, N. Berdunov, G. Mariotto, and S. Murphy, *Formation of the strain-induced electronic superstructure on the magnetite (111) surface*, Europhys. Lett. 63(6) (2003), pp. 867–873.
[31] N. Berdunov, S. Murphy, G. Mariotto, and I.V. Shvets, *Room temperature study of a strain-induced electronic superstructure on a magnetite (111) surface*, Phys. Rev. B 70(8) (2004), 085404.
[32] R. Pentcheva, F. Wendler, H.L. Meyerheim, W. Moritz, N. Jedrecy, and M. Scheffler, *Jahn–Teller stabilization of a 'polar' metal oxide surface: Fe_3O_4 (001)*, Phys. Rev. Lett. 94 (2005), 126101.
[33] R.S. Cutting, C.A. Muryn, D.J. Vaughan, and G. Thornton, *Substrate-termination and H_2O-coverage dependent dissociation of H_2O on Fe_3O_4 (111)*, Surf. Sci. 602(6) (2008), pp. 1155–1165.
[34] N. Mulakaluri, R. Pentcheva, M. Wieland, W. Moritz, and M. Scheffler, *Partial dissociation of water on Fe_3O_4 (001): Adsorbate induced charge and orbital order*, Phys. Rev. Lett. 103(17) (2009), 176102.